Mesostructured Crystalline Ceria with a Bimodal Pore System Using Block Copolymers and Ionic Liquids as Rational Templates

Torsten Brezesinski,† Christian Erpen,† Ken-ichi Iimura,‡ and Bernd Smarsly*,†

Max Planck Institute of Colloids and Interfaces, Am Mühlenberg 1, D-14476 Potsdam-Golm, Germany, and Department of Applied Chemistry, Faculty of Engineering, Utsunomiya University, 7-1-2 Yoto, Utsunomiya 321-8585, Japan

Received November 30, 2004. Revised Manuscript Received January 19, 2005

A concept is shown to fabricate mesoporous ceria thin films with a crystalline framework and a bimodal pore size distribution by evaporation-induced self-assembly followed by a suitable temperature treatment and template removal strategy. The use of a suitable block copolymer ($(CH_2CH_2CH_2(CH)CH_2CH_3)_{79}(OCH_2CH_2)_{89}OH$), "KLE") and an ionic liquid template (leading to pores 3 nm in diameter) generated a bimodal pore system of deformed spherical mesopores of ca. 6 nm × 16 nm with the smaller pores being located in the matrix between the larger ones. The porosity was studied by a combination of quantitative SAXS analysis, physisorption, AFM, and TEM, introducing a general methodology for a quantitative structural characterization of such films.

Introduction

The fabrication of mesoporous materials composed of metal oxides has attracted significant attention owing to their diverse properties (e.g., optical, electronic, magnetic). Within the huge family of binary and ternary metal oxides, ceria is of particular interest due to extraordinary thermal and chemical stability, which makes the system promising for catalysis. Also, in certain applications ceria acts as an oxygen storage or oxygen ion conductor.[1]

Recently, various working groups[2] as well as our group[3] have reported on the fabrication of mesoporous titania, ceria, and perovskite films with a long-range order of mesopores by the so-called evaporation-induced self-assembly (EISA) in combination with sol−gel processing. Using a novel block copolymer (the synthesis is described in detail in ref 3a), for the first time mesoporous ceria was obtained with an almost fully crystalline framework between well-defined mesopores, associated with a high degree of preferred orientation of deformed pores with respect to the surface.[4] Furthermore, sorption measurements revealed a surface area of 100−150 m^2/g, demonstrating the accessibility of the pores.

While various studies have focused on fabrication of binary oxides with one type of mesopore, very few efforts have been devoted to fabrication of hierarchical mesopore morphologies with small pores distributed within the walls of the corresponding larger ones. In general, such hierarchical pore systems are supposed to be more suitable for most potential applications than monomodal, mesoporous materials.[5] First, introduction of hierarchy in the pore system leads to a higher surface area, facilitating an enhanced interaction with adsorbents, and second, hierarchical pore structures allow for better macroscopic transport in the matrix. It is noteworthy that most of the mesoporous materials which reach technological applications possess bimodal pore structures. Prominent examples are bimodal silica pore structures obtained from spinodal demixing of polymers.[6] Bi- or even trimodal porous silicas with macropores and one or two types of well-defined mesopores have been prepared using colloidal polymeric particles as porogens for macropores and surfactants to generate mesopores between the macropores.[7]

* To whom correspondence should be addressed. E-mail: smarsly@mpikg.mpg.de.
† Max Planck Institute of Colloids and Interfaces.
‡ Utsunomiya University.

(1) (a) Lundberg, M.; Skarman, B.; Cesar, F.; Reine Wallenberg, L. *Microporous Mesoporous Mater.* **2002**, *54*, 97. (b) Terribile, D.; Trovarelli, A.; Llorca, J.; de Leitenburg, C.; Dolcetti, G. *J. Catal.* **1998**, *178*, 299. (c) Wang, J. A.; Dominguez, J. M.; Montoya, A.; Castillo, S.; Navarrete, J.; Moran-Pineda, M.; Reyes-Gasga, J.; Bokhimi, X. *Chem. Mater.* **2002**, *14*, 4676. (d) Lyons, D. M.; Ryan, K. M.; Morris, M. A. *J. Mater. Chem.* **2002**, *12*, 1207.

(2) (a) Haseloh, S.; Choi, S. Y.; Mamak, M.; Coombs, N.; Petrov, S.; Chopra, N.; Ozin, G. A. *Chem. Commun.* **2004**, *13*, 1460−1461. (b) Choi, S. Y.; Mamak, M.; Coombs, N.; Chopra, N.; Ozin, G. A. *Adv. Func. Mater.* **2004**, *14*, 335−344. (c) Grosso, D.; Soler-Illia, G. J. D. A.; Crepaldi, E. L.; Cagnol, F.; Sinturel, C.; Bourgeois, A.; Brunet-Bruneau, A.; Amenitsch, H.; Albouy, P. A.; Sanchez, C. *Chem. Mater.* **2003**, *15*, 4562. (d) Soler-Illia, G. J. D. A.; Crepaldi, E. L.; Grosso, D.; Sanchez, C. *Curr. Opin. Colloid Interface Sci.* **2003**, *8*, 109. (e) Yu, K.; Smarsly, B.; Brinker, C. J. *Adv. Func. Mater.* **2003**, *13*, 47−52. (f) Smarsly, B.; Xomeritakis, G.; Yu, K.; Liu, N. G.; Fan, H. Y.; Assink, R. A.; Drewien, C. A.; Ruland, W.; Brinker, C. J. *Langmuir* **2003**, *18*, 7295−7301. (g) Yu, K.; Hurd, A. J.; Eisenberg, A.; Brinker, C. J. *Langmuir* **2001**, *17*, 7961−7965. (h) Wu, X.; Yu, K.; Brinker, C. J.; Ripmeester, J. *Langmuir* **2003**, *19*, 7289−7294. (i) Yu, K.; Wu, X.; Brinker, C. J.; Ripmeester, J. *Langmuir* **2003**, *19*, 7282−7288.

(3) (a) Thomas, A.; Schlaad, H.; Smarsly, B.; Antonietti, M. *Langmuir* **2003**, *19*, 4455. (b) Smarsly, B.; Grosso, D.; Brezesinski, T.; Pinna, N.; Boissière, C.; Antonietti, M.; Sanchez, C. *Chem. Mater.* **2004**, *16*, 2948. (c) Grosso, D.; Boissière, C.; Smarsly, B.; Brezesinski, T.; Pinna, N.; Albouy, P. A.; Amenitsch, H.; Antonietti, M.; Sanchez, C. *Nat. Mater.* **2004**, *3*, 787.

(4) Brezesinski, T.; Groenewolt, M.; Pinna, N.; Antonietti, N.; Smarsly, B. *New J. Chem.* **2005**, *29*, 237−242.

(5) Rolison, D. R. *Science* **2003**, *299*, 1698−1701.

(6) (a) Nakanishi, K.; Kobayashi, Y.; Amatani, T.; Hirao, K.; Kodaira, T. *Chem. Mater.* **2004**, *16*, 3652−3658. (b) Ninnai, H.; Nakanishi, K.; Nishikawa, Y.; Yamanaka, J.; Hashimoto, T. *Langmuir* **2001**, *17*, 619−625. (c) Smatt, J. H.; Spliethoff, B.; Rosenholm, J. B.; Linden, M. *Chem. Commun.* **2004**, *19*, 2188−2189.

10.1021/cm0479180 CCC: $30.25
Published on Web 03/04/2005

However, so far very few studies have addressed the generation of crystalline oxides with well-defined bimodal pore structures on the mesoscale (2−50 nm), which is interesting from a general conceptual point of view and also regarding applications, where high porosities are needed (ZrO_2, CeO_2, etc.), especially in catalysis. While the fabrication of monomodal, crystalline, mesoporous oxides already imposes certain difficulties, the main problem in the preparation of bimodal, crystalline mesopore structures is related to the collapse of small mesopores due to stress arising from crystallization of the matrix. Using sol−gel templating followed by a thermal treatment, a fine balance is required to avoid structural collapse of the pore system.

A general methodology to obtain crystalline metal oxides with bimodal mesopore morphologies (with the small mesopores being located in the walls, surrounding the larger pores) is the use of appropriate amphiphilic templates of different sizes,[8] which are optimized with respect to the self-aggregation strength, thermal stability, and mixing behavior. Under the applied templating conditions the two surfactants have to be compatible with respect to their cohesion energies to avoid phase separation, which would be the normal behavior for surfactant mixtures. Recently, we demonstrated that a novel block copolymer ("KLE") has turned out to possess significantly better templating properties compared to other surfactants such as Pluronics.[9] For the smaller mesopores ionic surfactants should be suitable templates. However, it has to be emphasized that from a general thermodynamic point of view the creation of hierarchical micellar systems is usually unfavorable: in the majority of cases the block copolymer micelles and ionic surfactant aggregates either phase separate or form compound micelles. Recently, the mixing behavior of the KLE template with ionic surfactants was studied in detail by Hellweg et al.[10] It was demonstrated by dynamic light scattering, neutron scattering, and other techniques that in aqueous solutions common ionic surfactants such as SDS, etc., formed compound ("mixed") micelles with KLE. The size of these micelles was observed to be significantly decreased compared to pure KLE micelles. In consequence, combination of KLE and standard ionic surfactants (CTAB, SDS, etc.) cannot be expected to lead to the generation of hierarchical, micellar, and corresponding pore structures but would result in phase separation or the preferential formation of a single, mixed micellar phase. A corresponding behavior was previously described for non-ionic surfactants.[11] Several strategies have been reported to circumvent these problems. For instance, Antonietti et al. used small fluorinated co-templates to create bimodal mesoporous silica, taking advantage of the special templating properties of these surfactants.[12] It was demonstrated that in a certain concentration interval indeed the larger and smaller mesopores formed an "alloy"-like hierarchical mesopore structure. However, as a main difficulty in these and other studies it was shown that the small surfactant could only be added in a certain concentration range without observing phase separation. In contrast, ionic liquids (ILs) can be expected to be suitable candidates[7,13] because they were shown to be ideal templates to form small mesopores, especially as a co-template to obtain a hierarchical silica mesopore structure with KLE.[9] It was demonstrated for silica that indeed the IL template allowed the generation of high concentrations of small cylindrical mesopores of ca. 2.5−3 nm in the wall between the KLE mesopores.[9] Moreover, the size of the KLE mesopores was almost not affected by the presence of the IL. The special templating behavior of ionic liquids was attributed to the strong polarizability of the headgroup, thus leading to a stronger tendency for self-aggregation.[13c] Therefore, it can be expected that ionic liquids are also more suitable for the fabrication of crystalline, mesoporous materials compared to other ionic templates such as CTAB. As a further main advantage, some ILs (like the one used here) are industrial compounds and cheaper than specially designed surfactants (like the one in ref 12).

The scope of the present study is to present a general route for the preparation of such materials, aiming at a fundamental understanding of the involved crystallization processes and mesopore formation, especially addressing the special templating behavior of an ionic liquid in the presence of a block copolymer template. Furthermore, the present study is focused on a thorough characterization by various techniques to obtain a complete understanding of the porosity and crystallinity of these films. TEM, SAXS in symmetric reflection, nitrogen sorption, and AFM were used to determine the pore sizes and study the mesostructure. It is evident that the fabrication of crystalline thin films with a bimodal pore structure requires the application and development of suitable analytical techniques to allow for a meaningful characterization. Taking into account the low quantities of material, the combination of several independent techniques is inevitable in order to get an unambiguous characterization. Since a significant degree of shrinkage perpendicular to the surface is usually observed in mesoporous, amorphous, and crystalline films,[2g,i] which consequently leads to deformation of the pore shape, appropriate techniques had to be applied to determined the pore size in the direction parallel and

(7) (a) Zhou, Y.; Antonietti, M. *Chem. Commun.* **2003**, *20*, 2564−2565. (b) Sen, T.; Tiddy, G. J. T.; Casci, J. L.; Anderson, M. W. *Angew. Chem., Int. Ed*. **2003**, *42*, 4649−4653. (c) Antonietti, M.; Berton, B.; Goltner, C.; Hentze, H. P. *Adv. Mater.* **1998**, *10*, 154.

(8) (a) Tian, B.; Liu, X.; Zhang, Z.; Tu, B.; Zhao, D. *J. Solid State Chem*. **2002**, *167*, 324−329. (b) Song, M. G.; Kim, J. Y.; Cho, S. H.; Kim, J. D. *Langmuir* **2002**, *18*, 6110−6115. (c) Suzuki, K.; Ikari, K.; Imai, H. *J. Am. Chem. Soc*. **2004**, *126*, 462−463. (d) Sun, J.; Shan, Z.; Maschmeyer, T.; Moulijin, J. A.; Coppens, M. O. *Chem. Commun*. **2001**, 2670−2671. (e) Yuan, Z.; Blin, J.; Su, B. *Chem. Commun*. **2002**, 504−505. (f) Suzuki, K.; Ikari, K.; Imai, H. *J. Mater. Chem*. **2003**, *13*, 1812−1816. (g) Smatt, J. H.; Schunk, S.; Linden, M. *Chem. Mater*. **2003**, *15*, 2354−2361. (h) Huerta, L.; Guillem, C.; Latorre, J.; Beltran, A.; Beltran, D.; Amoros, P. *Chem. Commun*. **2003**, 1448−1449.

(9) Kuang, D.; Brezesinski, T.; Smarsly, B. *J. Am. Chem. Soc.* **2004**, *126*, 10543−10544.

(10) (a) Hellweg, T.; Dewhurst, C. D.; Eimer, W.; Kratz, K. *Langmuir* **2004**, *20*, 4330−4335. (b) Nordskog, A.; Fütterer, T.; von Berlepsch, H.; Böttcher, C.; Heinemann, A.; Schlaad, H.; Hellweg, T. *Phys. Chem. Chem. Phys*. **2004**, *6*, 3123−3129. (c) Nordskog, A.; Egger, H.; Findenegg, G. H.; Hellweg, T.; Schlaad, H.; von Berlepsch, H.; Böttcher, C. *Phys. Rev. E* **2004**, *68* (011406), 1−14..

(11) Smarsly, B.; Polarz, S.; Antonietti, M. *J. Phys. Chem. B* **2001**, *105*, 10473−10483.

(12) Groenewolt, M.; Antonietti, M.; Polarz, S. *Langmuir* **2004**, *18*, 7811−7819.

(13) (a) Zhou, Y.; Antonietti, M. *Chem. Mater.* **2004**, *16*, 544−550. (b) Zhou, Y.; Antonietti, M. *Adv. Mater*. **2003**, *15*, 1452−1455. (c) Antonietti, M.; Kuang, D. B.; Smarsly, B.; Yong, Z. *Angew. Chem., Int. Ed.* **2004**, *43*, 4988−4992. (d) Smarsly, B.; Kuang, D.; Antonietti, M. *Colloid Polym. Sci.* **2004**, *282*, 892−900.

perpendicular to the films. In particular, a suitable evaluation approach was developed for the SAXS of the oriented spherical KLE mesopores, providing the pore size normal to the substrate, complementing physisorption analysis. The approach extends an evaluation approach for randomly oriented spherical mesopores, which was introduced recently.[14] The lateral extension of the KLE mesopores and the homogeneity of the films were studied by detailed AFM investigations. The changes in crystallinity (as a function of the templates and heat treatment) were investigated by WAXS. Thereby, this study introduces a general methodology for a comprehensive characterization of mesoporous thin films on the level of the nanocrystals and the pore hierarchy.

Experimental Section

Materials. Cerium(III) chloride hydrate was received from Sigma-Aldrich and used as inorganic precursor. A block copolymer based on PEO and hydrogenated polybutadiene, ($H(CH_2CH_2$-$CH_2(CH)CH_2CH_3)_{79}(OCH_2CH_2)_{89}OH$),[3a] herein referred to as KLE, and an ionic liquid (1-hexadecyl-3-methylimidazolium chloride), IL,[9] both prepared with high purity in our lab, were used as templates to produce large and small mesopores, respectively.

Generation of Films. An ethanolic solution of KLE (75 mg) and IL (50 mg) was added to the precursor solution containing 875 mg of $CeCl_3 \cdot 7H_2O$, 200 mg of H_2O, and 8.0 g of EtOH. The resulting sol was stirred for 1 h before it was used. The mesoporous ceria films were prepared by dip coating silicon or glass substrates at constant withdrawal speed (6 mm/s) and constant relative humidity (8−14%). To guarantee a good optical quality after dip coating, it was necessary to transfer films to an oven at 80−100 °C (mechanism of suppression of local crystallization of cerium(III) chloride hydrate). Finally, the bimodal material was obtained through controlled nanocrystallization provided by heating with a ramp of 5 °C/min under air up to 400 °C. Potential leftover surfactant templates (KLE) were removed by solvent extraction with EtOH using a Soxhlet device.

Analytical Methods. Small- and wide-angle X-ray scattering were performed using a D8 diffractometer from Bruker Instruments (wavelength 0.154 nm). The X-ray photoelectron spectroscopy (XPS) measurements were taken on a Physical Electronics ESCA 5600 spectrometer with a monochromatic Al Kα X-ray source at a power of 400 W. The ETOA (θ) to the sample surface was adjusted to 45°. Spectra were obtained for both high-resolution mode (pass energy of 58.70 eV) for C1s, O1s, and Ce 3d and low-resolution mode (pass energy of 187.85 eV). Binding energies for the high-resolution spectra were calibrated by setting C1s at 284.6 eV. Gaussian−Lorentzian curves and Shirley background were applied for peak analysis.

Transmission electron microscopy (TEM) images were taken with a Zeiss EM 912Ω at an acceleration voltage of 120 kV, whereas a Philips CM200 FEG microscope equipped with a field emission gun was used for high-resolution transmission electron microscopy (HRTEM). Samples were ground in a ball mill and taken up with acetone. One droplet of the suspension was applied to a 400 mesh carbon-coated copper grid and left to dry. Sorption measurements were carried out at 77 K using Autosorb-1 from Quantachrome instruments. Tapping mode atomic force microscopy (AFM) images were recorded with a multimode AFM from Vecco Instruments employing Olympus microcantilevers (resonance frequency, 300 kHz; force constant, 42 N/m).

Theory of the SAXS in Symmetric Reflection of Oriented Spherical Mesopores. The ceria films were studied in detail by small-angle X-ray scattering in symmetric reflection (SRSAXS). The principal experimental setup of SRSAXS is illustrated in Scheme 1 (see ref 15).

Scheme 1. Schematic Representation of SAXS Measurements in Symmetric and Asymmetric Reflection

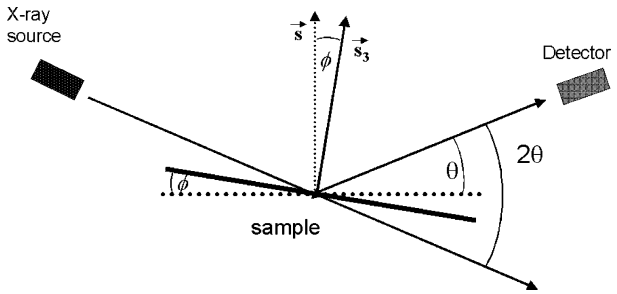

The SRSAXS data were extensively analyzed in order to determine the pore size and wall thickness. Due to the preferred orientation of the mesostructure, it is important to mention that the values obtained from this analysis only reflect the geometry in the z-(s_3)-direction, while no information can be obtained regarding the lateral dimension.

It was demonstrated in our recent studies that the mesostructure of thin films obtained from the KLE polymers corresponds to a bcc structure in [110] orientation with respect to the surface. Hence, the observed reflections (see Figure 4) can be assigned to (110) and (220) of the bcc mesostructure. The underlying idea of our evaluation approach is to analyze the experimental data by scattering functions corresponding to a reasonable structure model. These functions are described by geometric parameters, in particular the average pore radius R_{av}, its variance σ_R, the average long period d_{110}, its variance σ_d, and the average stack height L. For the theoretical SAXS of finite stacks of oriented polydisperse spheres we follow the approaches for lamellar nanocomposite films and mesoporous powder materials.[14,15] A suitable SAXS approach to evaluate the scattering data of oriented polydisperse spheres is similar to the one presented in ref 14 and given by

$$I_{sphere}(s) \propto (\langle |F(s)|^2 \rangle + |\langle F(s) \rangle|^2 (|Z_{1D}|^2(s) - 1)) \qquad (1)$$

with $s = 2/\lambda \sin \theta$, $2\theta =$ the scattering angle, and $\lambda = 0.154$ nm. $\langle\rangle$ stands for number average. For the form factors F we have chosen the approach described in ref 14 using a gamma distribution for the size of the spheres. For the lattice factor Z_{1D} we use an approach for a 1D point lattice of finite extension L with periodicity d_{110}.[15] If the finite width of the interface between ceria and the micelles/pores cannot be ignored, a suitable approach is given by multiplying eq 1 by the function $H_z^2(s) = \exp(-2\pi d_z^2 s^2)$,[15] where d_z is the thickness of the interface boundary. Taking into account the absorption correction A and an additive constant background scattering I_B (e.g., from 3D density fluctuations in the nanodomains[15]), we obtain for the final fitting curve

$$I_{fit}(s) = kA(s)[I(s)_{sphere} H_z^2(s) + I_B] \qquad (2)$$

$A(s)$ was calculated according to ref 15 with a linear absorption coefficient estimated for crystalline ceria. k is a scaling constant. The expression in eq 2 was additionally corrected for the slit smearing of our in-house diffractometer. Experimental data were then fitted by eq 2 under variation of the structural parameters R_{av},

(14) Smarsly, B.; Goltner, C.; Antonietti, M.; Ruland, W.; Hoinkis, E. *J. Phys. Chem. B* **2001**, *105*, 831−840.

(15) Ruland, W.; Smarsly, B. *J. Appl. Crystallogr.* **2004**, *37*, 575.

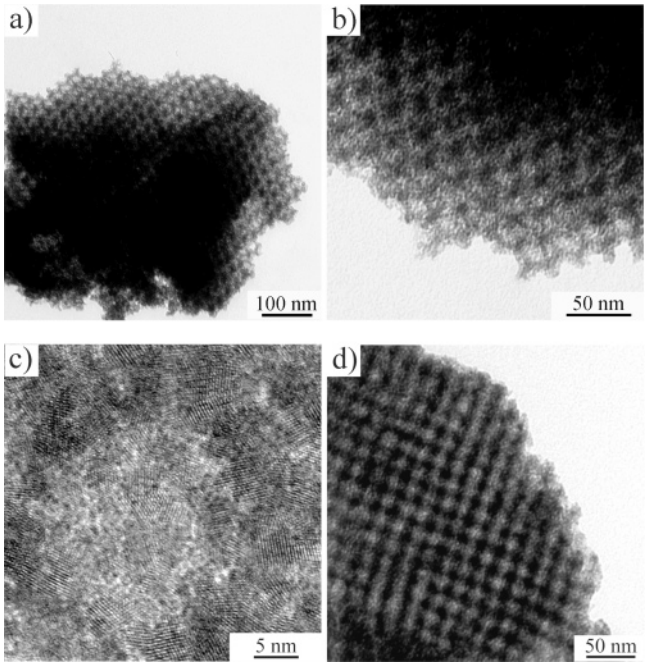

Figure 1. TEM images of bimodal ceria film (a, b) after temperature treatment at 300 °C and subsequent solvent extraction, corresponding HRTEM pattern (c) with a side length of 30 nm, showing a single mesopore, and TEM image (d) of a monomodal ceria system treated at 550 °C.

σ_R, d_{110}, σ_d, L, d_z, and I_B. The average wall thickness w (in the direction perpendicular to the film) is then given by $w = d_{110} - 2R_{av}$. d_z was set to 0.3 nm, corresponding to the approximate size of a CeO_2 unit.

Results and Discussion

TEM Study. Figure 1 shows TEM images of ceria films prepared using KLE (KLE-Ceria (d)) and KLE/IL (KLE/IL-Ceria (a, b)) as templates, indicating the high quality of the mesostructure, consisting of a long-range order of cubic arranged, spherical mesopores for both the bi- and the monomodal porous ceria system. Interestingly, the TEM patterns (a, b) depict the presence of two distinguishable types of pores of different sizes: compared to KLE-Ceria, the TEM image of KLE/IL-Ceria reveals a more inhomogeneous, granular matrix between the KLE mesopores. Similar TEM images were observed for bimodal, mesoporous silica obtained from templating with KLE and IL[9] and also mesoporous silica based on PS-*b*-PEO.[2e−i] The larger spherical pores can be attributed to KLE, and the wormlike, elongated pores located between them are due to the IL template, thereby excluding the possibility of phase separation into a KLE phase and domains enriched in IL. From these TEM micrographs we obtain a mesopore size of ca. 16−16.5 nm for KLE/IL-Ceria and an only slightly smaller value of ca. 14−14.5 nm for KLE-Ceria, while the small mesopores in KLE/IL-Ceria have an average size of about 2−3 nm. It is important to note that the specimen prepared for TEM break in the form of thin extended pieces due to the brittleness of the crystalline film, and therefore, in the TEM experiment the observer always looks in a direction perpendicular to the original film, thus observing extension of the mesostructure parallel to the film surface.

HRTEM of the same sample (Figure 1c) provides further insights into the constitution of the framework, showing a random orientation of small crystallites approximately 3 nm in size with small mesopores located between them. Also, the HRTEM analysis suggests an almost entirely crystalline framework without a significant content of amorphous regions. Selected area electron diffraction presents diffraction rings characteristic of a structure composed of small-sized, randomly oriented domains of crystallites.[4] Furthermore, the *d* spacings calculated from the diffraction rings match well with the cerianite structure and confirm the WAXS experiments (see below).

In conclusion, the TEM analysis suggests the following model for the pore structure of KLE/IL-Ceria and the distribution of the nanocrystals: in analogy to KLE-Ceria, the KLE mesopores form a bcc mesostructure, while the perfection is not affected by the presence of the ionic liquid. Even more, the presence of the IL seems to enhance the mesoscopic order, possibly through screening of the repulsion between the KLE micelles. More importantly, the small mesopores are located in the matrix between the KLE pores throughout the sample without phase separation, and additionally, TEM indicates that the mesopores are elongated with a diameter of 2−3 nm. The nanocrystals of ceria are about 3−4 nm in size, and therefore, it is evident that only 1−2 small mesopores have enough space in the matrix between two adjacent KLE mesopores. Since TEM itself probes local structural features and does not allow for an overall description of the material, further analytical techniques were applied to verify this structural model, Scheme 2.

Scheme 2. Illustration of the Templating of the KLE Block Copolymer (Red/Blue Spherical Micelles) and Ionic Liquid (Gray Distorted Cylinders)[a]

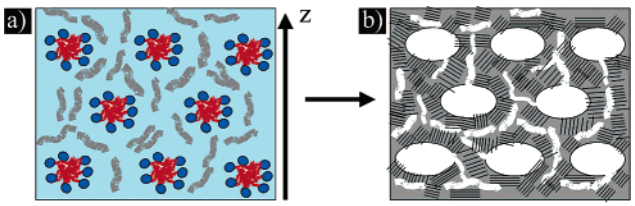

[a] (a) Mesostructure after solidification and (b) final bimodal, mesoporous structure with walls composed of crystalline cerium oxide (the small lamellar domains correspond to the nanocrystals, while the pores are white).

AFM Investigations. Besides TEM, atomic force microscopy (AFM) was used to further quantify the mesoporosity in these films (Figure 2a), showing a flat and crack-free surface, which proves that there is almost no horizontal contraction. More interestingly, AFM imaging reveals a regular pattern of maxima and minima, which correspond to the KLE mesopores, while the smaller mesopores are not visible by these AFM experiments, being embedded in the nanocrystals. Compared to SRSAXS and physisorption (see below), AFM provides information on the pore dimension and lattice parameter parallel to the film, which are important in light of film contraction parallel to the substrate. To the best of our knowledge, for the first time AFM was used to determine the real pore shape and size for mesostructured films with a cubic arrangement of pores. The height profile (Figure 2b), taken along a certain path of mesopores, indicates a high degree of lateral mesoscopic perfection. Furthermore, the height profile reveals that the pore-to-pore

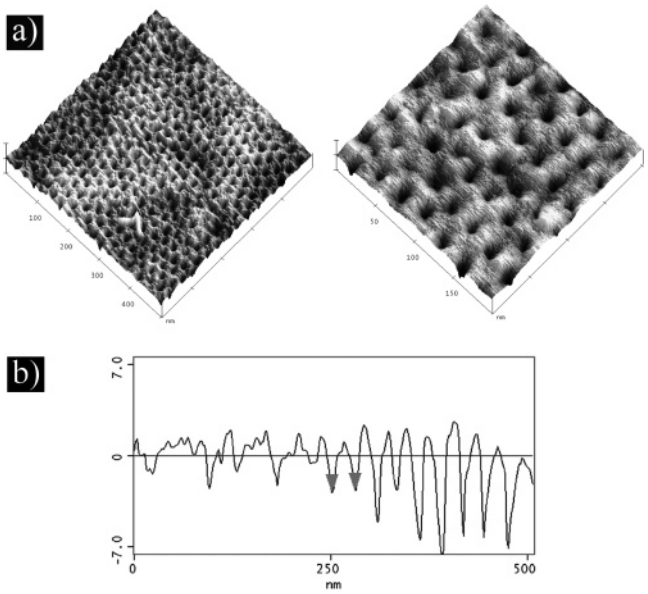

Figure 2. AFM images (a) recorded from the surface of a bimodal ceria film and the corresponding height profile (b). Both axes in b are in units of nm.

distance, depicted by the triangles, is always about the same size (approximately 28 nm), thereby confirming the mesostructural homogeneity. From this analysis the mesopore size of KLE/IL-Ceria was estimated to be around 15−16 nm and 13−14 nm for KLE-Ceria. These values are in good agreement with the corresponding TEM analyses. In addition, the AFM analysis is much more accurate in terms of absolute numbers of the pore and wall dimensions. It is important to emphasize that from AFM no macroscopic phase separation was observable.

Physisorption. Nitrogen sorption and water sorption measurements were used to characterize the porosity of KLE/IL-Ceria (see Figure 3). The bimodal, mesoporous CeO_2 was scratched from the Si-support, and IR spectroscopy (see Supporting Information) confirmed complete removal of the template by solvent extraction. The BET surface area was calculated to be 250−300 m^2/g (pore volume ca. 0.42 cm^3/g), thereby being significantly enhanced compared to the monomodal KLE-Ceria films (100−150 m^2/g, pore volume ca. 0.22 cm^3/g). Hence, the sorption data clearly demonstrate that both small and large mesopores are accessible. The theoretical porosities (taking into account the density of crystalline ceria), calculated on the basis of the amount of added surfactants, are 0.5 (KLE/IL-Ceria) and 0.2 cm^3/g (KLE-Ceria), thus slightly lower than the experimental ones, probably due to shrinkage. The adsorption branch shows two well-defined condensation steps which can be attributed to two different pore sizes. Consequently, the pore size distribution obtained from this branch (using the BJH approach) reveals two distinct maxima at ca. 3.8 and 6.7 nm (Figure 3b). It is evident to attribute these two pore sizes to the ionic liquid and the KLE block copolymer templates, respectively, suggesting a bimodal pore structure. For the monomodal, mesoporous KLE-Ceria films a mesopore size distribution is obtained, centered at 6.4 nm, almost identical to KLE/IL-Ceria. However, it has to be emphasized that from physisorption alone it would be not possible to exclude the possibility of phase separation during the self-assembly, that is into domains of mesostructured IL-Ceria and KLE-Ceria.

In Figure 3a the desorption branch is omitted because of nonequilibrium effects during the emptying of the pores (see Supporting Information). This unusual desorption behavior is partly attributable to the low quantity of material obtained from such films but also to the spherical mesopore shape. No difference was observed using very long equilibrium times (10 min per step) during desorption, suggesting further special sorption properties for this material. Nevertheless, desorption also reveals two separate pore-emptying steps for KLE/IL-Ceria. Also, it is worth noting that the desorption behavior is significantly different from that of KLE-Ceria (see Supporting Information), since for the latter sample the desorption closure point is located at even lower relative pressures. Hence, the presence of IL mesopores facilitates the emptying of the KLE mesopores, which supports the interpretation that the IL mesopores are located between the spherical KLE mesopores, while for KLE-Ceria the pore emptying can only occur through small cracks (micropores) in the ceria matrix. In this respect, our findings are in good agreement with the recent studies of Yu et al.[2e−i] Therein, it was demonstrated by various techniques (e.g., gas permeation, nitrogen sorption, and detailed TEM studies) that the connectivity of bcc mesopore structures in thin films, prepared from block copolymer templates with a similar procedure, is rather low and only established through a small number of micropores in the mesopore walls, similar to the KLE-Ceria. The unusual sorption behavior of the ceria films will be subject to a further detailed investigation.

To further elucidate the special features of the templating of IL/KLE mixed phases, films were prepared under similar

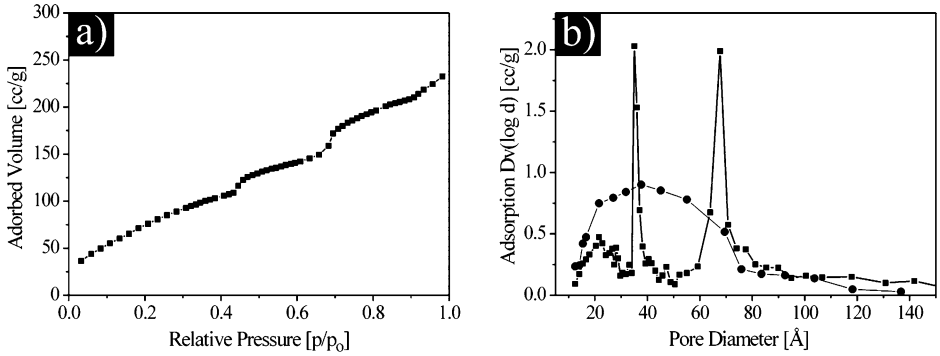

Figure 3. N_2 adsorption isotherm of bimodal ceria films (a) and the corresponding pore size distribution (b) of KLE/IL-Ceria (squares) and IL-Ceria (circles).

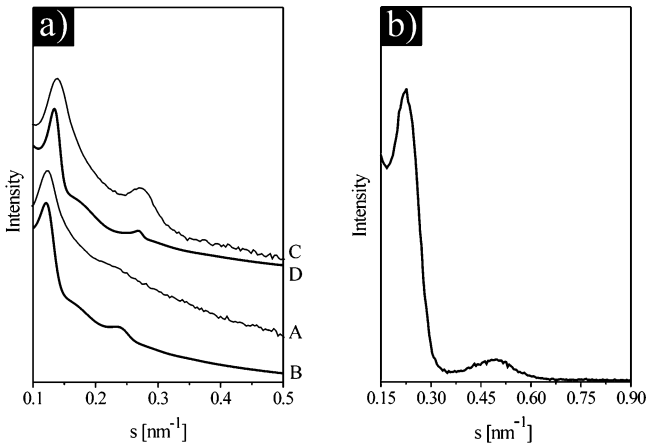

Figure 4. SRSAXS patterns (a) after annealing ceria films at 300 °C [(A) bimodal, mesoporous, crystalline ceria, (B) simulation of A, (C) monomodal, mesoporous, crystalline ceria, (D) simulation of C] and SRSAXS pattern (b) of IL-Ceria treated at 200 °C.

conditions using just the IL as template (IL-Ceria), also under variation of the IL/ceria ratio. It is seen that the material is highly nanocrystalline (Supporting Information) and highly porous (pore volume ca. 0.35 cm^3/g) and shows a large surface area (250−300 m^2/g), which represents an interesting material by itself, regarding the general goal to realize mesoporous, crystalline oxides with high porosities. In contrast to IL/KLE-Ceria, possessing a narrow distribution of pores around ca. 3 nm, in the case of IL-Ceria a quite broad pore size distribution is observed with pore sizes between 2 and 6 nm (Figure 3b). A similar behavior was frequently reported for the generation of mesoporous oxides using low molecular weight surfactants which, however, were only semicrystalline.[16] The partial pore collapse, indicated by the broad pore size distribution, can be attributed to the incompatibility of the pore size with the minimum size of the nanocrystals in the wall (ca. 3−4 nm). Thus, the bare physisorption results demonstrate that the presence of the KLE micelles/mesopores helps to maintain a stable bimodal pore framework with well-defined mesopore shapes and sizes.

SAXS Analysis. Small-angle X-ray scattering in symmetric reflection (SRSAXS) was used to obtain further insight into the mesostructure and mesoporosity. It was already reported recently that KLE-templated mesostructured films contain a bcc structure in [110] orientation with respect to the substrate.[3b] Using a 2D detector and GISAXS (grazing incidence SAXS) geometry it was demonstrated that a certain degree of mesophase contraction occurs perpendicular to the substrate, and only a minor lateral contraction was measurable. While SRSAXS probes the mesostructure only in the [110] direction and thereby ignores the lateral information, this type of measurement facilitates a more quantitative analysis of the scattering data compared to GISAXS. Figure 4a shows the SRSAXS data of samples KLE/IL-Ceria and KLE-Ceria. First, in both cases the presence of a sharp (110) reflection and even the second-order (220) interference proves the high mesostructural regularity of these crystalline materials. No interferences were observed corresponding to a periodic assembly of smaller IL mesopores, which is reasonable because the wall thickness of ca. 10 nm only allows for a short coherence length of the IL micelles/mesopores.

(16) (a) Liu, P.; Liu, J.; Sayari, A. *Chem. Commun.* **1997**, *6*, 577−578. (b) Antonelli, D. M. *Microporous Mesoporous Mater.* **1999**, *30*, 315−319.

Table 1. KLE Pore Size (nm) Obtained by Applied Methods, Revealing the Mesopore Dimension Parallel (D_{par}) and Perpendicular (D_{perp}) to the Substrate

	TEM (D_{par})	AFM (D_{par})	SRSAXS (D_{perp})	N2 adsorption (BJH approach)[a]
monomodal	14−14.5	13−14	6.1	6.4
bimodal	16−16.5	15−16	6.2	6.7

[a] Nitrogen adsorption probes an average value of the mesopore size, which is governed by the smaller dimension.

Second, as a main result, the position of the (110) interference is significantly shifted to smaller scattering vectors for KLE/IL-Ceria compared to KLE-Ceria. To decide if this change was due to an increase in the KLE mesopore dimension (in the [110] direction) or an increase in the matrix thickness between the mesopores, the SRSAXS data were subjected to a detailed quantitative analysis in terms of a structural model of spherical pores aligned onto a 1D lattice (see the theory discussion in the Experimental Section), ignoring the scattering from the smaller mesopores, which can be expected to contribute to a constant background scattering in the range of scattering vectors under study. From the fitting we obtain $d_{110} = 8.6$ nm and $R_{av} = 3.0$ nm ± 0.2 nm for KLE-Ceria and $d_{110} = 10.1$ nm and $R_{av} = 3.1$ nm ± 0.2 nm for KLE/IL-Ceria, in good agreement with the sorption analysis. Since the KLE-templated mesopores have the same size in KLE-Ceria and KLE/IL-Ceria, the change in the lattice parameter clearly suggests that the overall apparent pore wall thickness has increased due to incorporation of the ionic liquid template into the matrix between the KLE micelles. The interpretation that indeed the IL is located in the ceria matrix between the KLE micelles and does not phase separate into single domains is further supported by samples prepared using only the IL template. It is seen (Figure 4b) that the IL itself leads to a mesostructure under these conditions (heat treatment at 200 °C) using a IL/ceria ratio in a certain concentration range. The interference corresponds to the (10) and (20) reflections of an oriented 2D hexagonal lattice. Hence, for KLE/IL-Ceria, phase separation of an IL phase from the KLE domains should lead to measurable signals in SRSAXS.

Size and Shape of Larger Mesopores. The aforementioned analytical methods allow for a systematic comparison of the KLE pore sizes (Table 1). It highlights that the determination of the real pore size and shape requires the use of various techniques. In addition, it is noteworthy that the methods provide the same data for both directions with respect to the substrate, demonstrating their validity and accuracy for the present system.

WAXS Analysis. The WAXS experiments of KLE/IL-Ceria (Figure 5a) were performed after different annealing steps and mirror the expected crystallite sizes, as calculated by the Scherrer equation. The data reveal that crystallization into synthetic cerianite takes place at 300 °C and that no other phase is formed during temperature treatment. This

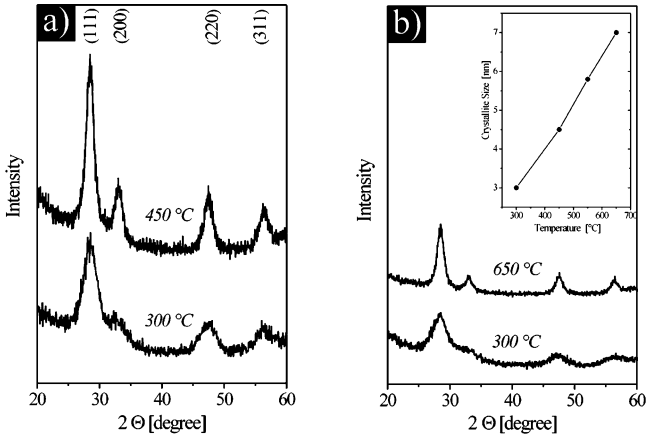

Figure 5. WAXS diffractograms (a) of KLE/IL-Ceria and (b) KLE-Ceria obtained after different calcination steps. (inset) Correlation of heat-treatment temperature and crystal size with respect to KLE-Ceria.

observation is in conformity with corresponding studies on mesoporous KLE-Ceria films (Figure 5b), revealing a linear correlation of the temperature treatment and crystal size for such systems.

However, incorporation of the IL into the ceria pore walls results in a significant change in the crystallization behavior: in the case of KLE-Ceria, it was possible to anneal the samples up to 650−700 °C without destroying the mesophase, leading to a crystal size of about 7 nm. In contrast, for KLE/IL-Ceria, at treatment above 400 °C significant distortions of the mesostructure were observed by SRSAXS (Supporting Information), attributable to the collapse of the IL mesopores between the KLE pores. Taking into account that the pore size templated by IL is around 3 nm, this observation is in good agreement with our recently introduced concept that the size of mesopores being surrounded by a matrix of nanocrystals has to be of the same order as the crystallites.[3b] Hence, the growth of nanoparticles beyond 3 nm (i.e., temperatures higher than ca. 400 °C) leads to the collapse of the IL-templated mesopores. Furthermore, we also studied the crystallization behavior of the IL-Ceria sample (Supporting Information). Similarly to KLE/IL-Ceria, these IL-Ceria samples are highly crystalline and have a crystallite size of around 3.5−4 nm at 300 °C (based on the Scherrer equation), increasing significantly up to 5 nm at 450 °C. Hence, in IL-Ceria and KLE/IL-Ceria the crystals grow faster upon temperature treatment compared to KLE-Ceria, leading to a severe distortion of the KLE mesophase in KLE/IL-Ceria, which in both cases can be attributed to a reorientation of the crystallites in the framework due to the mesostructural collapse of the IL mesopores. Moreover, these observations clearly demonstrate the crucial role of the temperature treatment during crystallization of mesostructured materials.

XPS Measurements. X-ray photoelectron spectroscopy was used to obtain detailed information on the oxidation state and distribution of corresponding cerium ions in mesostructured CeO_2 films. Figure 6 shows a characteristic Ce 3d spectrum, which is well known to be complex due to hybridization and partial occupancy of Ce 4f orbitals and O2p states. The full interpretation requires an extensive analysis of the obtained data, and therefore, the results were furthermore compared with previous investigations of ceria

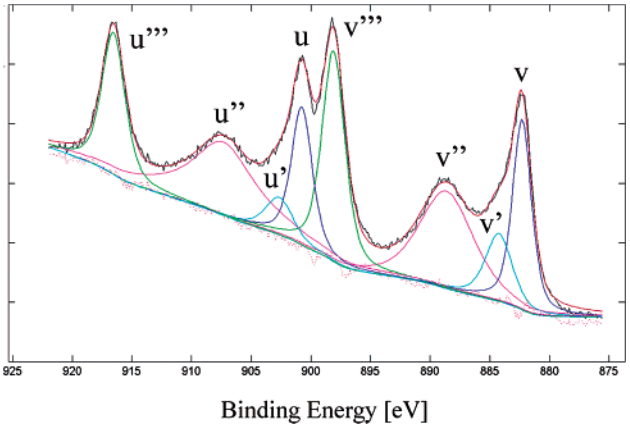

Figure 6. XPS Ce 3d spectrum of a mesostructured CeO_{2-x} film.

compounds.[17] This comparison showed that the binding energies of Ce 3d orbitals are in good agreement with literature values. Peaks labeled v, v″, and v‴ are attributable to Ce $3d^{5/2}$ photoemission lines of Ce^{4+}, while v′ is due to special configurations in Ce_2O_3.[17] The origin of the u structures (due to Ce $3d^{3/2}$) can be explained in the same way. According to ref 17, Ce_2O_3 produces XPS lines labeled v_0 and u_0 in the $3d^{5/2}$ and $3d^{3/2}$ regions, respectively. However, in our spectrum both peaks are negligibly small compared to other ones and are thus not shown in Figure 6.

It is known that Ce^{4+} can be partially reduced to Ce^{3+} during XPS experiments. The degree of ceria photoreduction, estimated by eq 3, is only about 8%, which is considerably smaller than that reported.[17]

$$Ce^{3+}(\%) = 100 \times \frac{\text{Area}(v_0) + \text{Area}(v') + \text{Area}(u_0) + \text{Area}(u')}{\sum(\text{Area}(v) + \text{Area}(u))} \quad (3)$$

It has been reported that the reduction takes place in the first few minutes of measurements, and thus, the photoreduction itself is inevitable when XPS is applied for chemical state evaluation of cerium oxides. In our case, taking account the smaller percentage of Ce^{3+} as well as no indication of impurities (e.g., Ce_2O_3) in WAXS patterns, we can infer that cerium exists almost exclusively as Ce^{4+} in the sample. To obtain information on the inner part of the film, an argon ion gun for depth profiling (Supporting Information) was used since XPS only provides information of the surface. The data point out slight shifts of binding energies with respect to the Ce 3d orbitals. One possible reason for peak shifting is a different chemical state (e.g., Ce^{3+}) depending on the depth from the surface, but for metal oxides, however, it is also known that Ar^+ bombardment induces selective removal of elements (preferential removal of oxygen (i.e., reduction) in most cases), resulting in a change of peak position as well as of chemical composition, which seems to be more probable. In conclusion, the XPS measurements

(17) (a) Romeo, M.; Bak, K.; El Fallah, J.; Le Normand, F.; Hilaire, L. *Surf. Interface Anal.* **1993**, *20*, 508. (b) Francisco, P. M. S.; Mastelaro, R. V.; Nascente, P. A. P.; Florentio, A. O. *J. Phys. Chem. B* **2001**, *105*, 10515−10522. (c) Silvestre-Albero, J.; Rodrígues-Reinoso, F.; Sepúlveda-Escribano, A. *J. Catal.* **2002**, *210*, 127−136. (d) Reddy, B. M.; Khan, A.; Yamada, Y.; Kobayahi, T.; Volta, J. C. *J. Phys. Chem. B* **2003**, *107*, 5162−5167.

are clearly indicative of a well-defined oxidation state of cerium(IV) oxide.

Conclusions

A strategy is presented which allows for the fabrication of crystalline cerium oxide thin films with a bimodal pore size distribution, showing an almost fully crystalline CeO_2 framework between the mesopores. The use of suitable templates, the KLE block copolymer, and an ionic liquid resulted in a system of deformed spherical mesopores of ca. 6 nm × 16 nm and wormlike pores ca. 2.5−3.0 nm in diameter between them using appropriate fabrication conditions. It is believed that the present study represents one of the first examples for a truly bimodal, mesoporous material with a crystalline framework, indicating that the present approach introduces a general methodology for tailoring such materials, as usually the preparation of such bimodal, mesoporous materials involves severe mesostructural collapse. Also, in most cases mixing of surfactants in sol−gel templating has been reported to lead to mixed micelles and thus to a monomodal pore size distribution, reflecting the average of the single templates. Hence, the special templating behavior of the KLE block copolymer family and ionic liquids seems to play a crucial role. The present work supports our recent study that the templates were compatible in the preparation of trimodal, porous silica and showed a stronger tendency for self-aggregation and a lower sensitivity toward distortions/stresses compared to other templates such as Pluronics or alkylammonium salts. In particular, use of an ionic liquid template seems to exceed the templating properties of standard surfactants in two respects: first, the IL template aggregates to wormlike micelles, tolerating the crystallization of ceria around them to a certain degree, which is in clear contrast to alkylammonium salts such as CTAB, which do not allow for fabrication of comparable bimodal, crystalline, porous materials. Second, the model proposed for the bimodal pore structure (see above) indicates a special interaction behavior of the IL with the KLE mesophase. On the basis of the aforementioned model for the distribution of IL and KLE, it is evident that the IL molecules form neither mixed micelles with KLE nor a separate phase. In contrast, the fact that the IL mesopores are located between the KLE mesopores suggests that the IL forms micelles (ad-micelles) adhering to the KLE micelles, which is in marked opposition to the interaction behavior of other surfactants with KLE. We speculate that the slight, measurable increase in the size of the KLE mesopores (16 vs 14−15 nm) in KLE/IL-Ceria compared to KLE-Ceria could be due to fusion of these ad-micelles with the KLE micelles during solidification of the matrix. The distinct templating properties of ionic liquids, already reported for silica,[9] therefore also hold true for mesoporous, crystalline materials. The special mixing behavior of this particular IL with KLE under templating conditions changes upon variation of the IL concentration. Adding significantly larger quantities of IL in the starting solutions (>60 mg in the starting solution, see above) indeed resulted in phase separation, while at any concentration below a hierarchical pore morphology could be achieved, which represents a substantially broader concentration range than in previous studies (see, e.g., ref 12). Although the present material could not be used at temperatures above 350 °C due to collapse of the small mesopores, it is remarkable that just the appropriate choice of templates enables the design of a well-defined bimodal pore morphology. Also, better temperature stability could be achieved relatively simple by doping with other metal salts, e.g., zirconium or samarium species. Future investigations will be devoted to a comparable study of other oxides such as titania.

Furthermore, the mesostructure of our ceria material confirms recent work on thin silica films with spherical mesopores arranged on a bcc lattice,[2e−i] which indicated that for this morphology the mesopores were almost isolated. In these studies the preparation involved evaporation-induced self-assembly of a block copolymer, and the low water content resulted in a retraction of the water-soluble PEO chains from the surrounding matrix, isolating the mesopores from each other. By contrast, the present study clearly proves that the mesopores are connected, which can be tuned by addition of the IL. Hence, our study is in agreement with the aforementioned studies in that the water content plays a crucial role with respect to the behavior of the PEO chains.

In addition, the present study introduces a general concept for the precise structural characterization of mesoporous thin films. Combination of various techniques such as SAXS in symmetric reflection, physisorption, TEM, and AFM provides a complete structural characterization of such materials, especially allowing for an exact determination of the degree of distortion of spherical pores. This concept is supposed to represent an invaluable tool to quantitatively characterize such coatings.

Acknowledgment. We thank Dr. Helmut Schlaad and Ines Below for the generous supply of the block copolymers and Dr. Daibin Kuang for the ionic liquid. Anne Heilig is acknowledged for the AFM measurements.

Supporting Information Available: IR spectra of the pure surfactant templates (IL,KLE) and KLE/IL-Ceria, WAXS diffractograms of IL-Ceria, nitrogen sorption isotherms of KLE-Ceria and KLE/IL-Ceria, nitrogen sorption isotherm of IL-Ceria, XPS spectra of the Ce 3d region, SAXS pattern of KLE/IL-Ceria, and ^{1}H NMR of the C16mimCl ionic liquid (PDF). This material is available free of charge via the Internet at http://pubs.acs.org.

CM0479180